

Heterogeneous Transparent Ultrathin Films with Tunable-Color Luminescence Based on the Assembly of Photoactive Organic Molecules and Layered Double Hydroxides

Dongpeng Yan, Jun Lu,* Min Wei,* Shenghui Qin, Li Chen, Shitong Zhang, David G. Evans, and Xue Duan

Multicolor luminescent films have great potential for use in optoelectronics, solid-state light-emitting materials, and optical devices. This work describes a systematic investigation of the ordered assembly of two- (blue/green, blue/orange, red/blue, red/green) and three-color (blue/red/green) light-emitting ultrathin films (UTFs) by using different photofunctional anions [bis(*N*-methylacridinium)@polyvinylsulfonate ion pairs and anionic derivatives of poly(*p*-phenylene), poly(phenylenevinylene), and poly(thiophene)] and Mg–Al-layered double hydroxide nanosheets as building blocks. The rational combination of luminescent components affords precise control of the emission wavelengths and intensity, and multicolored luminescent UTFs can be precisely tailored covering most of the visible spectral region. The assembly process of the UTFs and their luminescence properties, as monitored by UV–vis absorption and fluorescence spectroscopy, resulted in a gradual change in luminescence color in the selected light-emitting spectral region upon increasing the number of deposition cycles. X-ray diffraction demonstrates that the UTFs are periodic layered structures involving heterogeneous superlattices associated with individual photoactive anion–LDH units. These UTFs also exhibit well-defined multicolor polarized fluorescence with high polarization anisotropy, and the emissive color changes with polarization direction. Therefore, this work provides a way of fabricating heterogeneous UTFs with tunable-color luminescence as well as polarized multicolor emission, which have potential applications in the areas of light displays and optoelectronic devices.

1. Introduction

Multicolor luminescent materials^[1] have received extensive attention during the last two decades involving both fundamental studies and development of applications in light-emitting diodes, full-color displays, lasers, and optoelectronic devices. To date, although many multicolor emission materials

have been reported (semiconductor nano-crystals,^[2] rare-earth compounds,^[3] metal complexes,^[4] and polymers^[5]), several challenges remain unresolved. Firstly, the differences in luminous efficiency and intensity between different color components complicate the balance of the color display; as a result obtaining finely tunable luminescent colors is difficult and challenging. Secondly, a prerequisite for most optoelectronic applications is the development of transparent ordered films; unfortunately, such films have been much less frequently studied than solution and powder systems.^[6] Thirdly, efficient white-light-emitting phosphors for substituting conventional light sources are rather limited, owing to the complicated synthesis procedures involved.^[7a] Additionally, the energy/charge transfer processes occurring between the different color components make it difficult to finely control the color purity and stability of the resulting white light.^[7b] Furthermore, although white-light emissions have been observed using both organic^[7c] and inorganic materials,^[7d] white-light materials with special performance, such as polarized emission, for instance, are still very rare;

such materials need to be developed in order to solve the problems occurring in the backlighting of liquid-crystal displays.^[8] Therefore, to meet the requirements of future optical display devices, the development of new strategies or methodologies for fabricating multicolor light-emitting films and ultrathin film systems remains a major goal.

For the past two decades, π -conjugated polymers (π -CPs) and organic fluorescent dye molecules have been extensively studied,^[9] as their low cost, easy processing, high flexibility, and excellent luminescence properties give rise to many applications in optoelectronics. They have become a new generation of chromophores for use in large-area and plane displays. Furthermore, the combination of different luminescent compositions (such as red, green, and blue primary colors) also provides great opportunities for converting single-color emission into multicolor light-emitting materials and full-color displays. However,

D. P. Yan, Prof. J. Lu, Prof. M. Wei, S. H. Qin, L. Chen, S. T. Zhang, Prof. D. G. Evans, Prof. X. Duan
State Key Laboratory of Chemical Resource Engineering
Beijing University of Chemical Technology
Beijing, 100029, P. R. China
E-mail: lujun@mail.buct.edu.cn; weimin@mail.buct.edu.cn

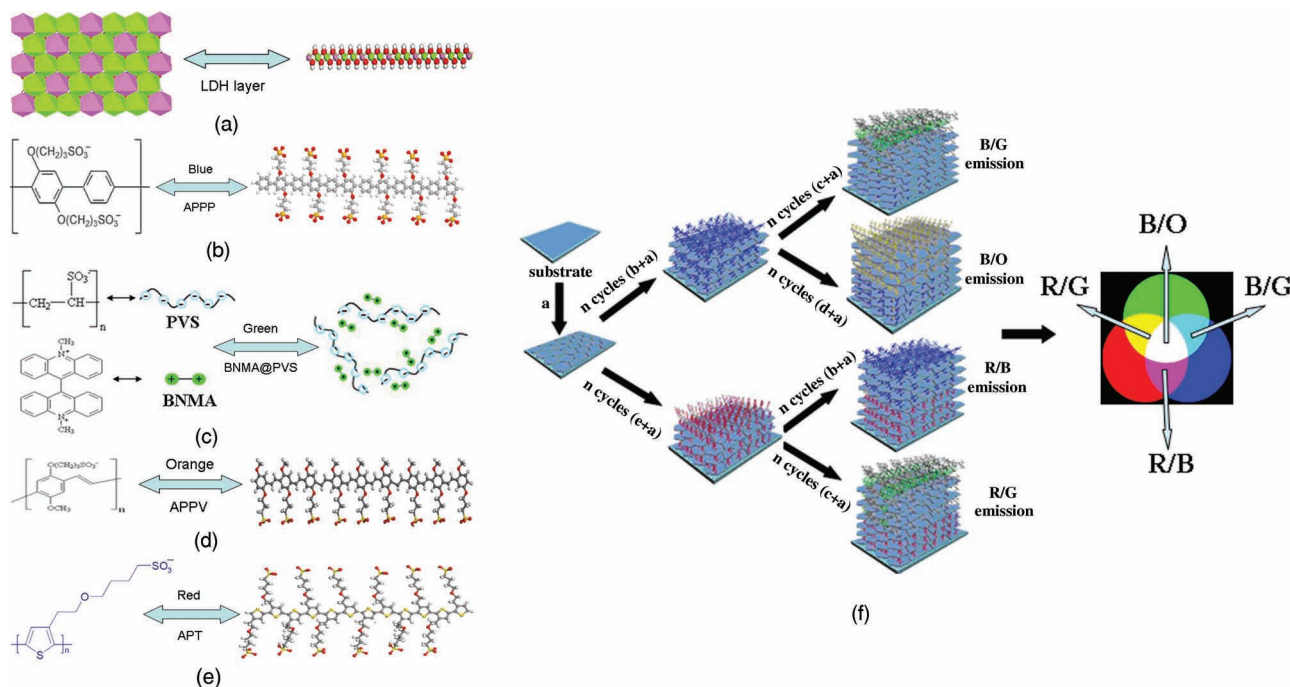
DOI: 10.1002/adfm.201002446

undesirable complications (such as energy transfer^[10a] and aggregation^[10b] between different luminescent components) often occur in tunable multicolor light-emitting materials based on organic luminescent systems. Moreover, the low thermal and optical stabilities of these organic dye and π -CP materials also lead to relatively short service lifetimes. One effective solution to these problems is the incorporation of luminescent guest molecules into an appropriate host matrix which can result in materials with physicochemical performances that are superior to those of the individual counterparts.^[11]

Layered double hydroxides (LDHs) are a large class of inorganic host materials that can be described by the general formula $[M^{II}_{1-x}M^{III}_x(OH)_2]^{z+}A^{n-}_{z/n} \cdot \gamma H_2O$, where M^{II} and M^{III} are divalent and trivalent metal ions respectively and A^{n-} is an anion. LDH materials feature a tunable layer charge density, variable elemental composition, and high chemical stability;^[12] the recent development of techniques for the delamination of LDH microcrystals into nanosheets has allowed the fabrication of ordered nanostructured thin films.^[12c,d,f,g] In our previous work, the layer-by-layer (LBL) assembly of luminescent organic anions and LDH nanosheets was employed to fabricate one type of ordered ultrathin film (UTF) with enhanced photoluminescent performance as well as high optical stability.^[13a] In addition, LDH-based UTFs with individual colors (red, green, blue) were obtained by the LBL process.^[13b-d] By combining the possibilities of electrostatic assembly and the three primary color principle it should be possible to fabricate multicolor luminescent UTF systems. Such luminescent anion/LDH UTFs should have the following advantages as multicolor luminescent materials: 1) the composition and loading of the luminescent

molecules can be precisely controlled through adjusting the assembly sequence, which facilitates the fine tuning of the multicolor light emission; 2) the LDH nanosheets provide the photoactive molecules with a rigid and ordered microenvironment, eliminating π - π stacking interactions and reducing the energy transfer between adjacent chromophores;^[13d] 3) the periodic ordered UTF systems may exhibit polarized multicolor luminescence, as a result of the orientation of the π -conjugated polymers in the 2D confined region of the LDH matrix with an intrinsic anisotropy.

To achieve a full-color luminescence display, in this work, a series of multicolor luminescent UTF materials (two-color: blue/green (B/G), red/blue (R/B), red/green (R/G) and blue/orange (B/O); three-color: red/blue/green (R/B/G) luminescent UTF) have been fabricated *via* the assembly of organic chromophores and LDH nanosheets. The basic building blocks for the anionic luminescent species are described elsewhere,^[13] namely sulfonated poly(*p*-phenylene) (APPP, blue photoemission, $\lambda_{max} = 410$ nm, Scheme 1b), sulfonated poly(*p*-phenylenevinylene) (APPV, orange photoemission, $\lambda_{max} = 550$ nm, Scheme 1d), and sulfonated poly(thiophene) (APT, red photoemission, $\lambda_{max} = 575$ nm, Scheme 1e). For green emission, the negatively charged cation@polyanion pair bis(*N*-methylacridinium) @polyvinylsulfonate (BNMA@PVS, green photoemission, $\lambda_{max} = 481$ nm, Scheme 1c) was selected. Mg-Al-LDH nanosheets were used as the positively charged building block (Scheme 1a), and the detailed assembly processes are illustrated in Scheme 1f. By varying the combination of individual chromophores, different colors covering most of the visible spectral region as well as white-light emission can be achieved in these UTF systems.



Scheme 1. a) Representation of one monolayer of Mg-Al-layered double hydroxide (Mg-Al-LDH) (dark pink: $Al(OH)_6$ octahedra; green: $Mg(OH)_6$ octahedra); the chemical formulae of: b) APPP (blue luminescence), c) BNMA@PVS (green luminescence), d) APPV (orange luminescence), and e) APT (red luminescence); f) the typical procedure for assembling two-color emitting UTFs with blue/green, blue/orange, red/blue, and red/green luminescence.

The as-obtained UTFs also present a long-range ordered structure and high anisotropy of the multicolor fluorescence, owing to the preferential orientation of the chromophores in the LDH gallery. To the best of our knowledge, no heterogeneous UTFs endowed with both color-tuning luminescence and polarized emission have been reported prior to our work. Therefore, this work provides a viable methodology for fabricating full-color UTFs based on the incorporation of organic luminescent molecules into an inorganic 2D matrix, which can be potentially applied in multicolor displays, polarized luminescence, and white-light devices.

2. Results and Discussion

2.1. Assembly of the Multicolor Luminescent UTFs

Our strategy for fabricating heterogeneous multicolor luminescent UTFs involves the stepwise assembly of individual luminescent species and LDH nanosheets; by changing the chromophore, assembly sequence, and number of bilayers, different multicolor luminescent UTFs can be obtained (Scheme 1f). Using this method, the energy transfer between different photoactive molecules, which occurs if they are co-assembled within the same LDH interlayer gallery,^[12c] can be effectively inhibited. Moreover, the assembly method employed in this work also allows fine control over the chemical components and luminescence colors of the UTFs. We illustrate several UTFs with different luminescence colors in the following section.

2.1.1. (APPP/LDH)₁₂/(BNMA@PVS/LDH)_n UTFs for B/G Luminescence

The assembly process for B/G two-color luminescence involved the deposition of (BNMA@PVS/LDH)_n ($n = 1-6$) bilayers upon the as-prepared (APPP/LDH)₁₂ UTF, and was monitored by UV-vis absorption spectroscopy after each deposition cycle (Figure 1). It was observed that the intensity of the absorption band at around 262 nm attributed to BNMA correlates linearly with n (Figure 1a, inset), indicating a stepwise and regular film growth procedure. As shown in Figure 1b, the luminescence peak at 410 nm can be attributed to the pristine (APPP/LDH)₁₂ UTF ($n = 0$); the intensities of the broad fluorescence peaks at 481 and 504 nm of the (APPP/LDH)₁₂/(BNMA@PVS/LDH)_n UTFs display a monotonic increase with n . The fluorescence spectra of the as-prepared UTFs with different numbers of BNMA@PVS/LDH bilayers show no obvious emission shift when compared to the pristine BNMA solution and BNMA@PVS/LDH UTFs,^[13c] which indicates that there is no aggregation of BNMA throughout the assembly process. As a result, the (APPP/LDH)₁₂/(BNMA@PVS/LDH)_n UTFs maintain the spectral properties of the individual chromophores, and the combined luminescence can be obtained using a single excitation wavelength. Photographs of the UTFs in daylight (inset in Figure 1a) and under UV illumination (inset in Figure 1b) provide a visual verification of the optical transparency and highly luminescent brightness, respectively, of the UTFs. The color coordinate measurements demonstrate that the luminescence

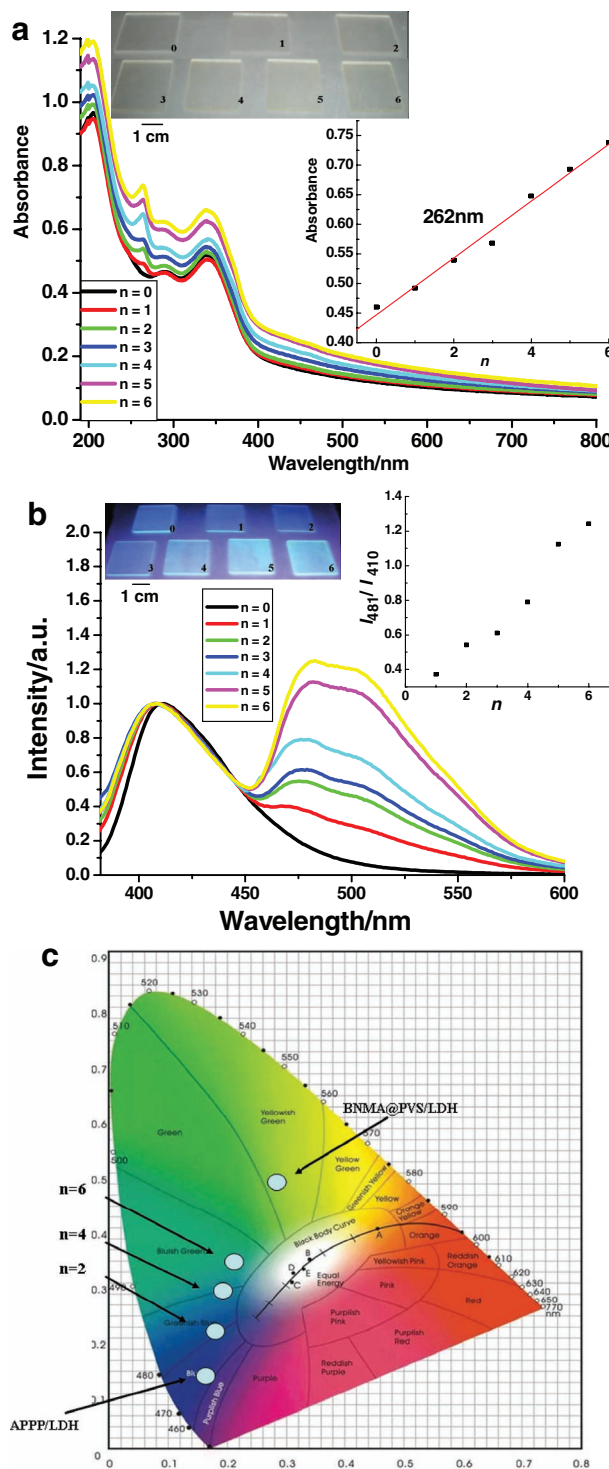


Figure 1. Optical spectroscopy characterization of the (APPP/LDH)₁₂/(BNMA@PVS/LDH)_n ($n = 0-6$) UTFs: a) UV-vis absorption spectra (the inset shows the plot of the intensity of the absorbance at 262 nm as a function of n); b) fluorescence spectra (the inset shows the ratio of the emission intensity at 481 nm to that at 410 nm); the photographs in (a) and (b) show the UTFs with different values of n in daylight and under UV light (365 nm), respectively. c) The change in color coordinates (the pristine BNMA@PVS/LDH UTF is populated at (0.336, 0.445)) with n .

color of the UTFs can be tuned from blue (Table S1 in the Supporting Information, CIE 1931: (0.172, 0.149); $n = 0$) to greenish-blue (CIE 1931: (0.189, 0.211); $n = 2$) and then to bluish-green (CIE 1931: (0.208, 0.343); $n = 6$) by simply changing the bilayer number of the green emitting units of BNMA@PVS/LDH (CIE 1931: (0.336, 0.445)). Therefore, tuning of the photoemission in the region from blue to green can be achieved by assembly of BNMA@PVS/LDH units onto the surface of APPP/LDH UTFs (Figure 1c).

2.1.2. (APPP/LDH)₁₂/(APPV/LDH)_n UTFs for B/O and White Luminescence

Enlightened by the principle that white-light emission can be constructed by a combination of blue and orange light in the correct ratio, we carried out the assembly of APPV/LDH bilayer units onto the (APPP/LDH)₁₂ UTF. UV-vis absorption spectroscopy (Figure 2a) showed that the intensity of the characteristic absorption band at around 439 nm (the π - π^* transition of APPV) increases linearly with n (Figure 2a, inset), indicating an ordered film growth. Moreover, in the fluorescence spectra of the (APPP/LDH)₁₂/(APPV/LDH)_n UTFs, the intensity of the sharp peak at around 550 nm also displays a consistent increase with n , as shown in Figure 2b. The ratio of the emission intensities of orange light to blue light can be varied from 0 to 1.1 by controlling the number of APPV/LDH bilayers. Therefore, the emission color of the (APPP/LDH)₁₂/(APPV/LDH)_n UTFs can be easily tuned. The change in luminescent color under UV irradiation as a function of the APPV/LDH bilayer number is displayed in the inset of Figure 2b; the luminescent color of the UTFs varies from blue ((APPP/LDH)₁₂ with CIE 1931: (0.172, 0.149)) to yellow ((APPP/LDH)₁₂/(APPV/LDH)₁₈ with CIE 1931: (0.405, 0.446), see Figure 2c and Table S2 in the Supporting Information). In particular, the luminescent color of the (APPP/LDH)₁₂/(APPV/LDH)₆ UTF is located within the white light region of the CIE 1931 diagram, and the color coordinates (0.296, 0.317) are close to the standard coordinates for white light (0.333, 0.333). This indicates the potential application of this system as a white luminescent source. Moreover, the as-prepared (APPP/LDH)₁₂/(APPV/LDH)_n UTFs showed no shift in the maximum photoemission for either APPP and APPV compared to the pristine APPP/LDH and APPV/LDH UTFs,^[13b] demonstrating that neither energy transfer between APPP and APPV nor chromophore aggregation occurs throughout the whole assembly process. These observations also indicate that the polymer chains are isolated from one another by the rigid LDH nanosheets, and the interlayer π - π stacking interactions as well as energy transfer are therefore effectively inhibited.

2.1.3. Other UTF Systems for R/B and R/G Luminescence

By adjusting the chromophore, deposition sequence, and ratio of the APPP/LDH, BNMA@PVS/LDH, and APT/LDH units with blue, green, and red luminescence, respectively, we have obtained other luminescent UTFs with finely tunable photoemissions in the visible spectral region: the (APPP/LDH)₁₂/(APT/LDH)_n, (APT/LDH)₁₂/(APPP/LDH)_n, and (APT/LDH)₁₂/(BNMA@PVS/LDH)_n systems have B/R, R/B, and R/G color emission, respectively. The detailed spectral characterization

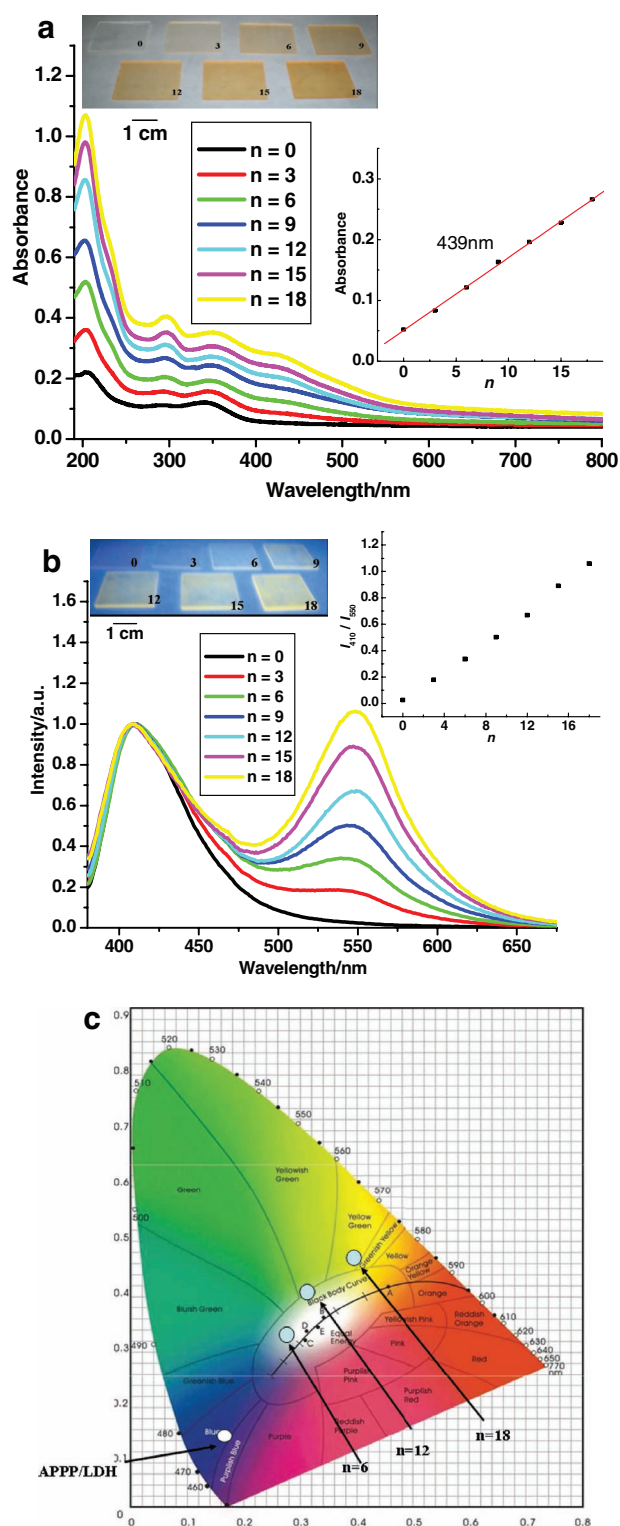


Figure 2. Optical spectroscopy characterization of the (APPP/LDH)₁₂/(APPV/LDH)_n ($n = 0$ –18) UTFs: a) UV-vis absorption spectra (the inset shows the plot of the intensity of the absorbance at 439 nm as a function of n); b) fluorescence spectra (the inset shows the ratio of emission intensity at 550 nm to that at 410 nm); the photographs in the inset of (a) and (b) show the UTFs with different values of n in daylight and under UV light (365 nm), respectively; c) variation in the color coordinates with increasing n .

of these UTF systems is described in the Supporting Information (Figures S1–S3; Tables S3–S5). It was also found that the tunable luminescence of the two-color UTFs is almost independent of the order in which each luminescent chromophore was assembled, demonstrating the universality and versatility of this approach.

To further compare the luminescent efficiency of the as-prepared UTFs with those fabricated by other methods, we also prepared double-color luminescent thin films containing the same organic compositions by a drop-casting technique.^[11c] The photoluminescent quantum yield (PQY) values of the LDH-based organic-inorganic hybrid UTFs are systematically higher than those of their drop-cast counterparts (see Supporting Information, Table S6), which indicates that the fluorescent quenching and/or energy transfer between two emissive molecules can be effectively reduced by the introduction of LDH nanosheets in these double-color luminescent samples.

2.2. Structural and Morphological Characterization of the Hybrid UTFs

X-ray diffraction was employed to detect the periodic structure of the two-color luminescent UTFs. It was found that all of the two-color UTF systems had two sets of periodic structure associated with ordered stacking arrangements of the two different luminescent species within the LDH nanosheets. For example, in the XRD pattern of the pristine (APPP/LDH)₁₂ UTF, a reflection at a 2θ value of 5° was observed, corresponding to the basal spacing of 2 nm associated with the superlattice structure of the APPP/LDH unit as described in our previous work.^[13a] As increasing numbers of BNMA@PVS/LDH units are deposited on the (APPP/LDH)₁₂ UTF, a new reflection at about 7° appears in addition to that of the APPP/LDH unit, and its relative intensity increases with n (shown in Figure 3a). In the case of the (APPP/LDH)₁₂/(APPV/LDH) _{n} UTFs, upon increasing the bilayer number of the APPV/LDH unit, a strong reflection at about 2.5 – 2.7° was observed, indicating that the UTFs possess

a periodic structure in the direction normal to the film with a period of 3.3–3.5 nm, which is close to that for the pristine APPV/LDH UTFs (ca. 3.5 nm).^[13b] Moreover, the peak intensity increases gradually with increasing n . Importantly, the relative intensity of the XRD reflection attributed to the APPP/LDH unit remains unchanged in the (APPP/LDH)₁₂/(APPV/LDH) _{n} UTFs, suggesting that the degree of order of the (APPP/LDH)₁₂ UTF does not change throughout the whole assembly process. Similar behavior was also observed for the other UTF systems (APPP/LDH)₁₂/(APT/LDH) _{n} , (APT/LDH)₁₂/(APPP/LDH) _{n} , and (APT/LDH)₁₂/(BNMA@PVS/LDH) _{n} (Figure S4 in the Supporting Information). Such ordered heterogeneous structure should facilitate the application of these UTFs in optical devices.

The surface morphology of the (APPP/LDH)₁₂/(APPV/LDH) _{n} UTFs was further studied by scanning electron microscopy (SEM) and atomic force microscopy (AFM) (Figure 4). The thickness and root-mean-square (RMS) roughness values of the as-prepared UTFs are listed in Table 1. Side-view SEM images (Figure 4a) show that the thickness of the UTFs with different numbers of bilayers can be estimated to be 29 ($n = 0$), 63 ($n = 9$), and 108 nm ($n = 18$); therefore, the average thickness of one bilayer of APPV/LDH can be estimated to be around 4 nm, which is close to the basal spacing observed by XRD (ca. 3.5 nm). This further confirms the uniform and periodic layered structure of the UTFs, and is also in agreement with the behavior revealed by absorption and fluorescence spectroscopy described above. Moreover, it can be seen from top-view SEM images with low and high resolution that the surface of the as-prepared UTFs is microscopically continuous and uniform (Figure 4b), with an RMS roughness of 9.3–11.7 nm over a $2\ \mu\text{m} \times 2\ \mu\text{m}$ area of the UTFs. Similar results were obtained for the other two-color UTF systems (Table 1, Figures S5–S8 in the Supporting Information), indicating that regular and smooth surfaces were retained throughout the fabrication process.

2.3. Two-Color Polarized Luminescent UTFs

The periodic structure of these luminescent UTFs further inspired us to exploit their polarized luminescence properties, and the glancing incidence geometry was employed to determine their luminescence anisotropy value r .^[14] Typical polarized photoemission spectra of the two-component UTFs for (APPP/LDH)₁₂/(APPV/LDH)₉ (B/O light emission) and (APPP/LDH)₁₂/(APT/LDH)₉ (B/R light emission) are displayed in Figure 5. In contrast to the single-color polarized emission in other systems,^[15] the anisotropy values for the two UTF systems are larger than 0.25 in the range from 400 to 650 nm (when comparing the directions parallel and perpendicular to the excitation polarization (I_{VV} vs. I_{VH}) for in-plane polarized excitation light). The results confirm that polarized luminescence in the visible region can be achieved for the as-prepared two-color luminescent UTFs. Moreover, the r values in the blue spectral region are larger than the highest theoretical value of 0.4 for a system lacking molecular macroscopic alignment and possessing absorption transition dipoles parallel to the emission one,^[16] indicating an ordered alignment of the π -CPs between the LDH nanosheets. By changing the polarization direction

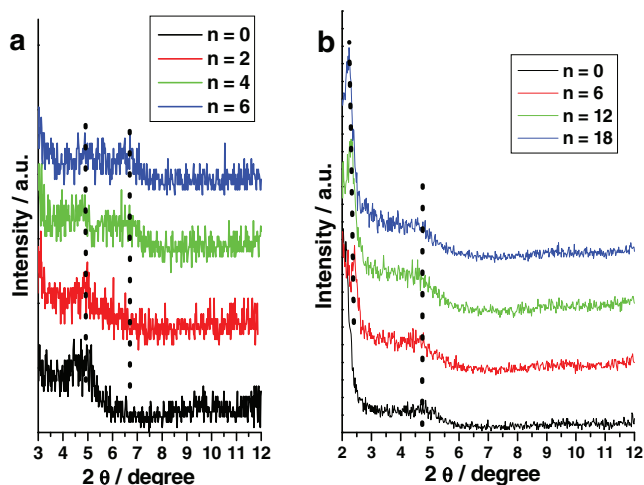


Figure 3. XRD patterns of a) the (APPP/LDH)₁₂/(BNMA@PVS/LDH) _{n} UTFs ($n = 0, 2, 4, 6$); b) the (APPP/LDH)₁₂/(APPV/LDH) _{n} UTFs ($n = 0, 6, 12, 18$).

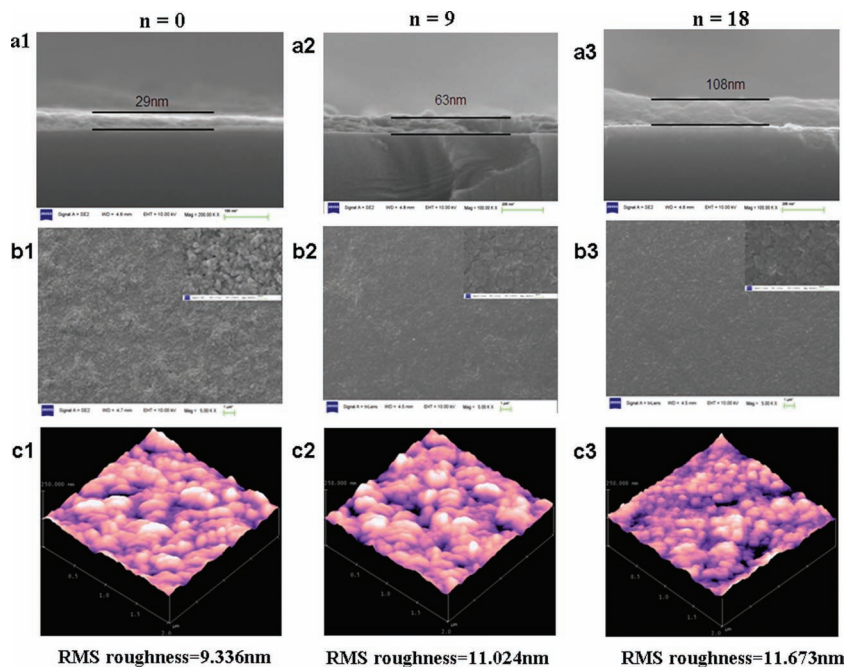


Figure 4. The morphology of $(\text{APPP/LDH})_{12}/(\text{APPV/LDH})_n$ UTFs ($n = 0, 9, 18$): a) side-view SEM images; b) top-view SEM images with low and high (inset) resolution; c) tapping-mode AFM topographical images.

of the as-prepared two-color UTFs with a single excitation wavelength, it was found that the intensity ratios for the two luminescence spectral regions were very different, suggesting that the relative intensities of the two luminescence colors and hence the overall emission color can be adjusted by changing the polarization direction. For the $(\text{APPP/LDH})_{12}/(\text{APPV/LDH})_9$ UTF, the ratio of the intensities of luminescence at 410 and 550 nm (I_{410}/I_{550}) was 1.25 for the I_{VV} polarization mode, whereas it was only 0.71 for the I_{VH} polarization mode (Figure 5a). In the case of the $(\text{APPP/LDH})_{12}/(\text{APT/LDH})_9$ UTF, the intensity ratio I_{410}/I_{575} had values of 1.65 (I_{VV} polarization mode) and 0.94 (I_{VH} polarization mode) (Figure 5b). The variation in intensity ratio with polarization mode is possibly associated with the orientation and arrangement of the photoactive molecules in the UTFs. We anticipate that these polarized luminescent UTFs can be applied as color-switchable film materials.

Furthermore, the effects of assembly sequence and bilayer number on the polarized luminescence of the UTFs were studied. Figures S9 and S10 in the Supporting Information show that the $(\text{APPP/LDH})_{12}/(\text{APT/LDH})_{12}$ and $(\text{APT/LDH})_{12}/(\text{APPP/LDH})_{18}$ UTFs exhibit similar luminescent anisotropy values to that of $(\text{APPP/LDH})_{12}/(\text{APT/LDH})_9$ described above, suggesting that the anisotropy of these UTFs is independent of both the bilayer number and assembly sequence. Other typical polarization characteristics of the two-color luminescent systems are shown in Figures S11–S13 (Supporting Information) for the $(\text{APPP/LDH})_{12}/(\text{BNMA@PVS/LDH})_n$ ($n = 3, 4$), $(\text{APPP/LDH})_{12}/(\text{APPV/LDH})_{18}$, and $(\text{APT/LDH})_{12}/(\text{BNMA@PVS/LDH})_n$ ($n = 3, 4$) UTFs, respectively. All these UTFs display well-defined polarized luminescence in the corresponding spectral region. Therefore, it can be concluded that photoactive molecule/LDH UTFs have well-oriented and uniform structures, consistent with the XRD and SEM observations. Macroscopic polarized luminescence is related to the ordered assembly of conjugated polymers with their 1D microscopic anisotropy and the LDH nanosheets with their 2D microscopic anisotropy. These UTFs can function as a new type of white and two-color polarized luminescent materials for optoelectronic devices.

2.4. Three-Color Luminescent UTFs

To further investigate the structure and luminescence performance of three-color luminescence systems based on the red, green, and blue luminescent building blocks, the assembly of UTFs containing APPP/LDH, BNMA@PVS/LDH, and APT/LDH units was performed. It was found that the small cation BNMA desorbs easily in the anionic π -CPs solution (see Figure S14 for the UV-vis and fluorescence spectra of the $(\text{APPP/LDH})_{12}/(\text{BNMA@PVS/LDH})_6/(\text{APT/LDH})_n$ UTFs), and as a result the assembly sequence is an important factor in the construction

Table 1. The thickness and RMS roughness of multicolor UTFs.

Multicolor UTFs	Thickness (nm)/RMS roughness (nm)		
	$n = 0$	$n = 9$	$n = 18$
$(\text{APPP/LDH})_{12}/(\text{APT/LDH})_n$	29 ^{a)} (24 ^{b)} /9.3	67 (58)/9.9	89 (87)/11.2
$(\text{APT/LDH})_{12}/(\text{APPP/LDH})_n$	43 ^{a)} (39 ^{b)} /9.8	62 (61)/10.3	87 (79)/9.3
$(\text{APPP/LDH})_{12}/(\text{APPV/LDH})_n$	29 ^{a)} (24 ^{b)} /9.3	63 (62)/11.0	108 (98)/11.7
	$n = 0$	$n = 3$	$n = 6$
$(\text{APPP/LDH})_{12}/(\text{BNMA@PVS/LDH})_n$	29 ^{a)} (24 ^{b)} /9.3	38 (37)/9.5	50 (52)/10.4
$(\text{APT/LDH})_{12}/(\text{BNMA@PVS/LDH})_n$	43 ^{a)} (39 ^{b)} /9.8	52 (47)/12.3	65 (51)/12.6

^{a)}Thickness obtained from the side-view SEM image; ^{b)}Thickness calculated from the XRD data.

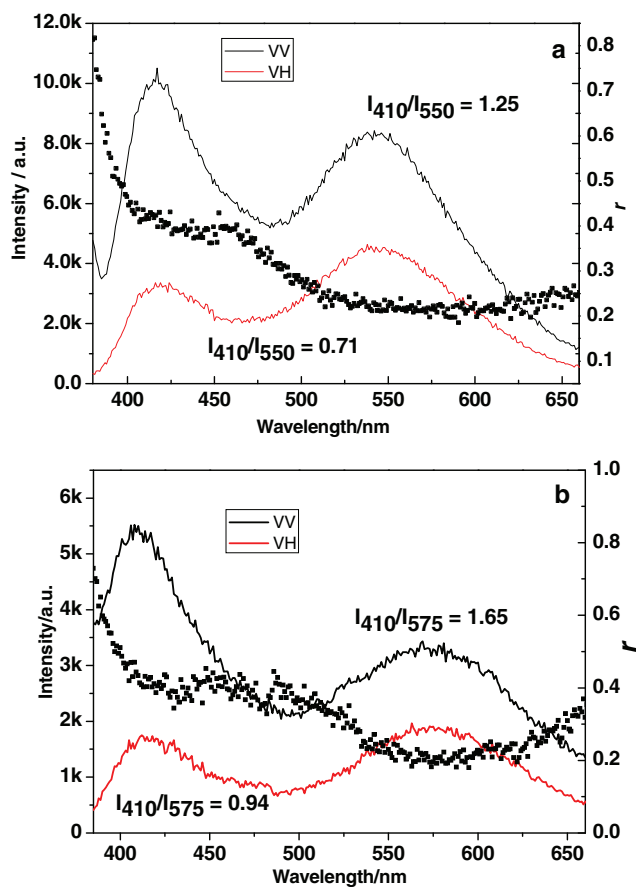


Figure 5. Polarized fluorescence profiles with glancing incidence geometry in the VV and VH modes and the anisotropy value (r) for two-color luminescent UTFs: a) the (APPP/LDH)₁₂/(APPV/LDH)₉ UTF; b) the (APPP/LDH)₁₂/(APT/LDH)₉ UTF.

of three-color luminescent UTFs. We chose a strategy whereby the BNMA@PVS/LDH bilayer unit is deposited onto the (APT/LDH)₁₂/(APPP/LDH)₁₂ UTF, giving a UTF denoted as (APT/LDH)₁₂/(APPP/LDH)₁₂/(BNMA@PVS/LDH)_{*n*} ($n = 0-12$). **Figure 6a** shows the UV-vis spectra of these materials, in which a linear increase in absorbance at 262 nm related to BNMA was observed with increasing number of bilayers of BNMA@PVS/LDH, indicating a regular assembly of the BNMA@PVS/LDH unit onto the as-prepared (APT/LDH)₁₂/(APPP/LDH)₁₂ UTF. Moreover, the fluorescence intensity ratio I_{523}/I_{410} increased with increasing number of bilayers of BNMA@PVS/LDH. The brightness of the green fluorescence observed upon UV irradiation showed a gradual increase with number of bilayers (shown in the inset of **Figure 6b**). The surface morphology of the resulting UTFs was investigated by SEM and AFM (**Figure 7a-c**). The thickness of the UTFs was found to vary from around 103 nm ($n = 6$) to 112 nm ($n = 12$). The RMS roughness of the UTFs ranged from 10.0–15.3 nm according to AFM measurements. Additionally, the XRD pattern for the (APT/LDH)₁₂/(APPP/LDH)₁₂/(BNMA@PVS/LDH)₁₂ UTF (**Figure 7d**) shows three reflections corresponding to the different components: APT/LDH (ca. 3°), APPP/LDH (ca. 5°) and BNMA@PVS/LDH (ca. 6.7°), demonstrating that the UTF retains a periodic superlattice structure throughout the whole assembly process.

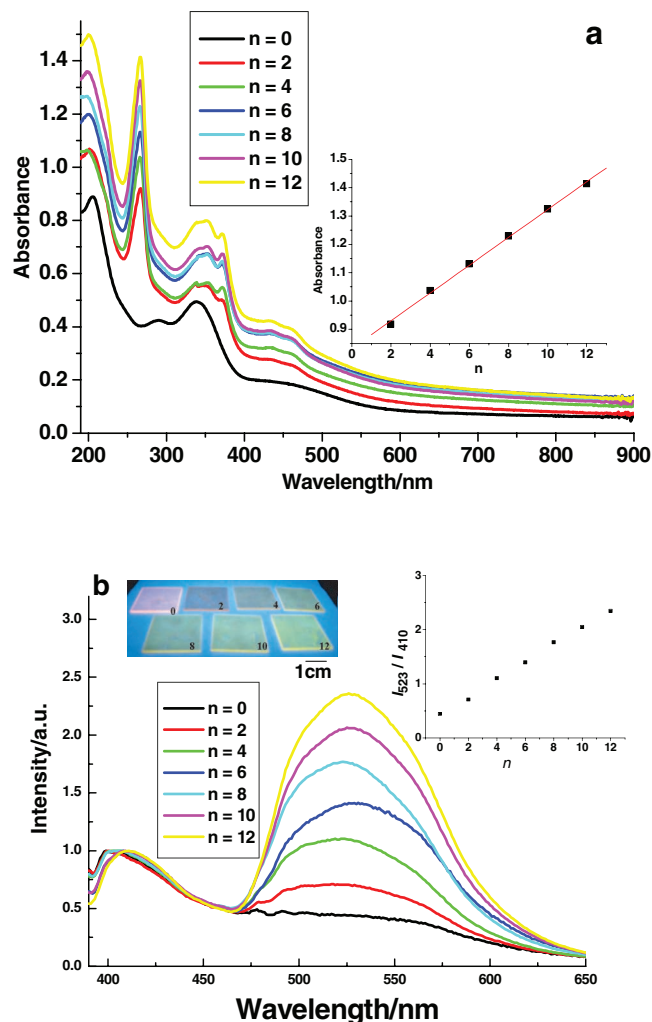


Figure 6. Optical spectroscopy characterization of the (APT/LDH)₁₂/(APPP/LDH)₁₂/(BNMA@PVS/LDH)_{*n*} ($n = 0-12$) UTFs: a) UV-vis absorption spectra (the inset shows the variation of absorbance at 262 nm as a function of n); b) fluorescence spectra (the inset shows the ratio of fluorescence intensity at 523 nm to that at 410 nm as a function of n); the photograph in (b) shows the images of UTFs with different bilayer numbers under UV light (365 nm).

3. Conclusion

A versatile and feasible LBL strategy has been developed for the fabrication of multicolor luminescent UTFs based on the combination of anionic photoactive species and positively charged LDH nanosheets. The luminescence color of the resulting hybrid UTFs can be easily tuned over nearly the whole visible spectrum by rational selection of the R/G/B color photoemissive building blocks. The UTFs exhibit a periodic long-range heterogeneous structure, uniform morphology, and controllable film thickness on the nanometer scale. Furthermore, well-defined multicolor polarized luminescence with high anisotropy was observed for these UTFs, which may facilitate both fundamental research and technological applications in multicolor or white polarized photoemission devices. For example, these heterogeneous UTFs can act as a possible color conversion layer of

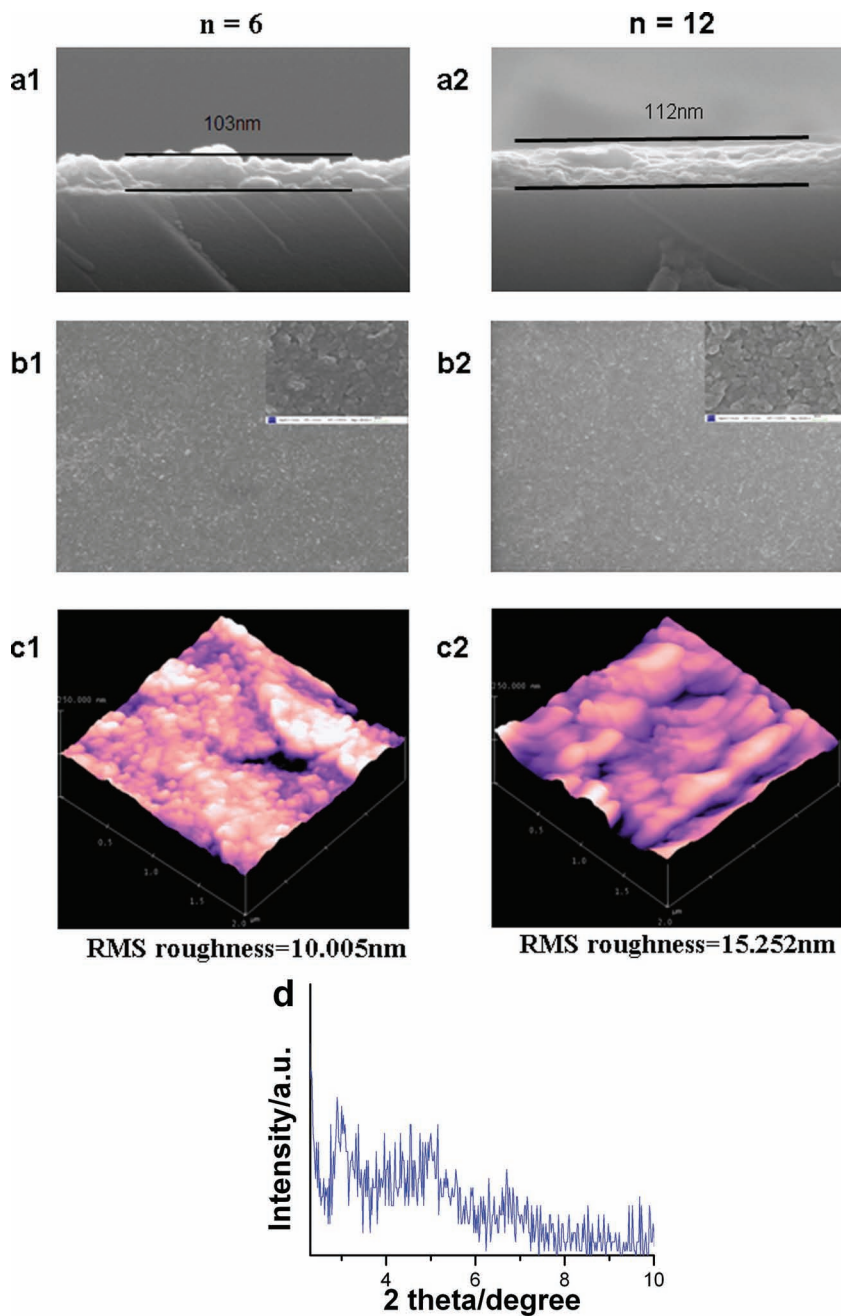


Figure 7. The morphology of the $(\text{APT/LDH})_{12}/(\text{APPP/LDH})_{12}/(\text{BNMA@PVS/LDH})_n$ UTFs: a) side-view SEM images; b) top-view SEM images with low and high resolution; c) tapping-mode AFM topographical images; d) XRD pattern for the $(\text{APT/LDH})_{12}/(\text{APPP/LDH})_{12}/(\text{BNMA@PVS/LDH})_{12}$ UTF.

flat-panel displays in lighting devices. Our method for the fabrication of light-emitting materials possesses several advantages compared with conventional synthesis techniques, such as component variability, low cost, and easy manipulation. Importantly, by virtue of the three primary color principle, the same LBL assembly strategy can be extended and employed to fabricate other luminescent systems. We anticipate that multicolor photoemission with any desired color in the visible region can be obtained by accurately tuning the assembly component unit,

sequence, and cycle number, which facilitates potential applications of these UTFs in multicolor light displays, lasers, and optoelectronic devices.

4. Experimental Section

Reagents and Materials: Poly(2,5-bis(3-sulfonatopropoxy)-1,4-phenylene, disodium salt-*alt*-1,4-phenylene) (APPP), potassium poly(5-methoxy-2-(3-sulfopropoxy)-1,4-phenylenevinylene) (APPV), bis(*N*-methylacridinium) nitrate (BNMA), and polyvinylsulfonate potassium salt (PVS) were purchased from Sigma Chemical Co. Ltd. Sodium poly(2-(3-thienyl)ethoxy-4-butylsulfonate) (APT) was purchased from American Dye Source, Inc. Analytical grade $\text{Mg}(\text{NO}_3)_2 \cdot 6\text{H}_2\text{O}$, $\text{Al}(\text{NO}_3)_3 \cdot 9\text{H}_2\text{O}$, and urea were purchased from Beijing Chemical Co. Ltd. and used without further purification.

Fabrication of the Two- and Three-Color Luminescent UTFs: The synthesis process and exfoliation of Mg-Al-LDH were similar to that described in our previous work.^[13a] 0.1 g of Mg-Al-LDH was shaken in 100 cm³ of formamide solution for 24 h to produce a colloidal suspension of exfoliated Mg-Al-LDH nanosheets. A quartz glass substrate was cleaned in concentrated $\text{NH}_3/30\% \text{H}_2\text{O}_2$ (7:3) and then concentrated H_2SO_4 for 30 min each, followed by thorough washing with deionized water. The detailed assembly of the pristine $(\text{APPP/LDH})_n$, $(\text{APPV/LDH})_n$, $(\text{APT/LDH})_n$, and $(\text{BNMA@PVS/LDH})_n$ UTF units have been described elsewhere.^[13] Fabrication of the two- or three-color luminescent UTFs involved the alternate deposition of one type of luminescent UTF onto the surface of a different as-prepared luminescent UTF. By controlling the deposition sequence and number of layer-by-layer cycles, multicolor UTFs with different luminescence were obtained. Taking the $(\text{APPP/LDH})_{12}/(\text{APPV/LDH})_n$ UTFs with B/O photoemission as a typical example, the as-prepared $(\text{APPP/LDH})_{12}$ UTF with APPP as the top layer was dipped into a colloidal suspension ($1 \text{ g} \cdot \text{dm}^{-3}$) of LDH nanosheets for 10 min and then washed thoroughly. The resulting UTF was immersed into 100 mL of APPV aqueous solution (0.025 wt.%) for another 10 min and then washed. Multilayer films of $(\text{APPP/LDH})_{12}/(\text{APPV/LDH})_n$ were fabricated by alternate deposition into a suspension of LDH nanosheets and a solution of APPV for n cycles. The resulting films were dried under a nitrogen gas flow for 2 min at 25 °C. Other two-color systems were constructed by a similar process. The three-color luminescent UTFs $(\text{APT/LDH})_{12}/(\text{APPP/LDH})_{12}/(\text{BNMA@PVS/LDH})_n$ ($n = 0-12$) were fabricated by alternate assembly of BNMA@PVS and LDH nanosheets onto the as-prepared $(\text{APT/LDH})_{12}/(\text{APPP/LDH})_{12}$ UTF. For comparison, the double-color luminescent thin films only containing the organic compositions were prepared by a drop-casting method, and the deposition sequence and the concentration of the solutions are the same as for the corresponding UTFs.

Characterization: UV-vis absorption spectra were collected in the range of 190 to 900 nm on a Shimadzu U-3000 spectrophotometer, with a slit width of 1.0 nm. The fluorescence spectra were recorded on a Shimadzu RF-5301PC spectrofluorometer with an excitation source of 360 nm, illuminating the UTF at an incidence angle of 45°. Both the

excitation and emission slits were set to be 3 nm. Steady-state polarized photoluminescence measurements of the as-prepared UTFs were carried out with an Edinburgh Instruments FLS 920 spectrofluorometer. The CIE 1931 color coordinates of the fluorescence were determined using a Photo Research PR-650 SpectraScan colorimeter with the detector vertical to the surface of the UTF. X-ray diffraction patterns (XRD) were recorded using a Rigaku 2500VB2+PC diffractometer under the following conditions: 40 kV, 50 mA, Cu K α radiation ($\lambda = 0.154056$ nm) using step-scanning in steps of 0.04° (2θ) in the range from 2 to 10° using a count time of 10 s/step. The morphology of the thin films was investigated using a scanning electron microscope (SEM Zeiss Supra 55) equipped with an EDX attachment (EDX Oxford Instruments Isis 300), at an applied accelerating voltage of 20 kV. The surface roughness and thickness data were obtained by using atomic force microscopy (AFM) software (Digital Instruments, Version 6.12).

Supporting Data: Color coordinates for the (APPP/LDH) $_{12}$ /(BNMA@PVS/LDH) $_m$, (APPP/LDH) $_{12}$ /(APPV/LDH) $_m$, (APPP/LDH) $_{12}$ /(APT/LDH) $_m$, (APT/LDH) $_{12}$ /(APPP/LDH) $_n$ and (APT/LDH) $_{12}$ /(BNMA@PVS/LDH) $_n$ UTFs: see Table S1–S5, respectively. Photoluminescent quantum yield (PQY) values of the UTFs: see Table S6. Optical spectroscopy characterization for the (APPP/LDH) $_{12}$ /(APT/LDH) $_m$, (APT/LDH) $_{12}$ /(APPP/LDH) $_m$ and (APT/LDH) $_{12}$ /(BNMA@PVS/LDH) $_n$ UTFs: see Figure S1–S3, respectively. Low-angle XRD patterns for the (APPP/LDH) $_{12}$ /(APT/LDH) $_m$, (APT/LDH) $_{12}$ /(APPP/LDH) $_m$ and (APT/LDH) $_{12}$ /(BNMA@PVS/LDH) $_n$ UTFs (Figure S4). The morphology of the (APPP/LDH) $_{12}$ /(BNMA@PVS/LDH) $_m$, (APPP/LDH) $_{12}$ /(APT/LDH) $_m$, (APT/LDH) $_{12}$ /(APPP/LDH) $_m$ and (APT/LDH) $_{12}$ /(BNMA@PVS/LDH) $_n$ UTFs: see Figures S5–S8, respectively. Photoemission profiles with VV and VH polarizations and the anisotropy value (r) for the (APPP/LDH) $_{12}$ /(APT/LDH) $_{12}$, (APT/LDH) $_{12}$ /(APPP/LDH) $_{18}$, (APPP/LDH) $_{12}$ /(BNMA@PVS/LDH) $_m$, (APPP/LDH) $_{12}$ /(APPV/LDH) $_{18}$, and (APT/LDH) $_{12}$ /(BNMA@PVS/LDH) $_n$ UTFs: see Figure S9–S13, respectively. Optical spectroscopy characterization of the (APPP/LDH) $_{12}$ /(BNMA@PVS/LDH) $_6$ /(APT/LDH) $_n$ UTFs: see Figure S14.

Supporting Information

Supporting Information is available from the Wiley Online Library or from the author.

Acknowledgements

We gratefully acknowledge Prof. R. Friend, Prof. W. Jones, A. Kumar, and R. Gymer from the University of Cambridge for the helpful discussions and measurements of the luminescent quantum yields. This work was supported by the National Natural Science Foundation of China, the 111 Project (Grant No.: B07004), and the 973 Program (Grant No.: 2011CBA00504).

Received: November 19, 2010

Published online: May 4, 2011

- [1] a) A. H. Mueller, M. A. Petruska, M. Achermann, D. J. Werder, E. A. Akhador, D. D. Koleske, M. A. Hoffbauer, V. I. Klimov, *Nano Lett.* **2005**, *5*, 1039; b) Y. Zhao, H. Gao, Y. Fan, T. Zhou, Z. Su, Y. Liu, Y. Wang, *Adv. Mater.* **2009**, *21*, 3165.
- [2] a) M. Kuang, D. Y. Wang, H. B. Bao, M. Y. Gao, H. Mohwald, M. Jiang, *Adv. Mater.* **2005**, *17*, 267; b) Y.-P. Ho, M. C. Kung, S. Yang, T.-H. Wang, *Nano Lett.* **2005**, *5*, 1693; c) P. O. Anikeeva, J. E. Halpert, M. G. Bawendi, V. Bulovic, *Nano Lett.* **2009**, *9*, 2532.
- [3] a) H. X. Mai, Y. W. Zhang, R. Si, Z. G. Yan, L. D. Sun, L. P. You, C. H. Yan, *J. Am. Chem. Soc.* **2006**, *128*, 6426; b) L. Y. Wang, Y. D. Li, *Nano Lett.* **2006**, *8*, 1645; c) F. Wang, X. G. Liu, *J. Am. Chem. Soc.* **2008**, *130*, 5642; d) Y. Yoon, B. Lee, K. S. Lee, H. Heo, J. H. Lee, S. Byeon, I. S. Lee, *Chem. Commun.* **2010**, *46*, 3654.
- [4] a) H. V. R. Dias, H. V. K. Diyabalanage, M. A. Rawashdeh-Omary, M. A. Franzman, M. A. Omary, *J. Am. Chem. Soc.* **2006**, *128*, 12072; b) G. J. Zhou, C.-L. Ho, W.-Y. Wong, Q. Wang, D. G. Ma, L. X. Wang, Z. Y. Lin, T. B. Marder, A. Beeby, *Adv. Funct. Mater.* **2008**, *18*, 499.
- [5] a) C.-L. Chiang, S.-M. Tseng, C.-T. Chen, C.-P. Hsu, C.-F. Shu, *Adv. Funct. Mater.* **2008**, *18*, 248; b) A. C. A. Chen, S. W. Culligan, Y. Geng, S. H. Chen, K. P. Klubek, K. M. Vaeth, C. W. Tang, *Adv. Mater.* **2006**, *16*, 783.
- [6] a) Y. Wang, Z. Y. Tang, M. A. Correa-Duarte, L. M. Liz-Marzán, N. A. Kotov, *J. Am. Chem. Soc.* **2003**, *125*, 2830; b) Y. L. Lei, Q. Liao, H. B. Fu, J. N. Yao, *J. Am. Chem. Soc.* **2010**, *132*, 1742; c) Y. Yoon, S. Byeon, I. S. Lee, *Adv. Mater.* **2010**, *22*, 3272.
- [7] a) R. Abbel, C. Grenier, M. J. Pouderoijen, J. W. Stouwdam, P. E. L. G. Leclère, R. P. Sijbesma, E. W. Meijer, A. P. H. J. Schenning, *J. Am. Chem. Soc.* **2009**, *131*, 833; b) Y.-S. Park, J.-W. Kang, D. M. Kang, J.-W. Park, Y.-H. Kim, S.-K. Kwon, J.-J. Kim, *Adv. Mater.* **2008**, *20*, 1957; c) M. C. Gather, R. Alle, H. Becker, K. Meerholz, *Adv. Mater.* **2007**, *19*, 4460; d) C. X. Li, C. M. Zhang, Z. Y. Hou, L. L. Wang, Z. W. Quan, H. Z. Lian, J. Lin, *J. Phys. Chem. C* **2009**, *113*, 2332.
- [8] C. Weder, C. Sarwa, A. Montali, C. Bastiaansen, P. Smith, *Science* **1998**, *279*, 835.
- [9] a) J. Fraxedas, *Adv. Mater.* **2002**, *14*, 1603; b) A. Ajayaghosh, V. K. Praveen, *Acc. Chem. Res.* **2007**, *40*, 644.
- [10] a) S. R. Amrutha, M. Jayakannan, *J. Phys. Chem. B* **2008**, *112*, 1119; b) A. L. Igor, K. Jinsang, M. S. Timothy, *J. Am. Chem. Soc.* **1999**, *121*, 1466.
- [11] a) T.-Q. Nguyen, J. J. Wu, V. Doan, B. J. Schwartz, S. H. Tolbert, *Science* **2000**, *288*, 652; b) C. M. Carbonaro, A. Anedda, S. Grandi, A. Magistris, *J. Phys. Chem. B* **2006**, *110*, 12932; c) D. P. Yan, J. Lu, M. Wei, D. G. Evans, X. Duan, *J. Phys. Chem. B* **2009**, *113*, 1381; d) D. P. Yan, J. Lu, J. Ma, M. Wei, D. G. Evans, X. Duan, *Phys. Chem. Chem. Phys.* **2010**, *12*, 15085; e) D. P. Yan, J. Lu, J. Ma, M. Wei, S. Qin, L. Chen, D. G. Evans, X. Duan, *J. Mater. Chem.* **2010**, *20*, 5016; f) W. Y. Shi, Z. Y. Sun, M. Wei, D. G. Evans, X. Duan, *J. Phys. Chem. C* **2010**, *114*, 21070; g) D. P. Yan, J. Lu, J. Ma, M. Wei, D. G. Evans, X. Duan, *Angew. Chem.* **2011**, *123*, 746; *Angew. Chem. Int. Ed.* **2011**, *50*, 720.
- [12] a) A. M. Fogg, V. M. Green, H. G. Harvey, D. O'Hare, *Adv. Mater.* **1999**, *11*, 1466; b) J. H. Choy, S.-Y. Kwak, Y.-J. Jeon, J.-S. Park, *Angew. Chem.* **2000**, *112*, 4207; *Angew. Chem. Int. Ed.* **2000**, *39*, 4041; c) L. Li, R. Z. Ma, Y. Ebina, N. Iyi, T. Sasaki, *Chem. Mater.* **2005**, *17*, 4386; d) Z. P. Liu, R. Z. Ma, M. Osada, N. Iyi, Y. Ebina, K. Takada, T. Sasaki, *J. Am. Chem. Soc.* **2006**, *128*, 4872; e) G. G. Aloisi, U. Costantino, F. Elisei, L. Latterini, C. Natali, M. Nocchetti, *J. Mater. Chem.* **2002**, *12*, 3316; f) X.-X. Guo, F.-Z. Zhang, D. G. Evans, X. Duan, *Chem. Commun.* **2010**, *46*, 5197; g) S. Huang, X. Cen, H. D. Peng, S. Z. Guo, W. Z. Wang, T. X. Liu, *J. Phys. Chem. B* **2009**, *113*, 15225.
- [13] a) D. P. Yan, J. Lu, M. Wei, J. B. Han, J. Ma, F. Li, D. G. Evans, X. Duan, *Angew. Chem.* **2009**, *121*, 3119; *Angew. Chem. Int. Ed.* **2009**, *48*, 3073; b) D. P. Yan, J. Lu, M. Wei, J. Ma, D. G. Evans, X. Duan, *Langmuir* **2010**, *26*, 7007; c) D. P. Yan, J. Lu, L. Chen, S. H. Qin, J. Ma, M. Wei, D. G. Evans, X. Duan, *Chem. Commun.* **2010**, 5912; d) D. P. Yan, J. Lu, M. Wei, J. Ma, D. G. Evans, X. Duan, *AIChE J.* **2011**, DOI: 10.1002/aic.12400.
- [14] a) D. P. Yan, J. Lu, M. Wei, J. Ma, D. G. Evans, X. Duan, *Chem. Commun.* **2009**, 6358; b) D. P. Yan, S. H. Qin, L. Chen, J. Lu, J. Ma, M. Wei, D. G. Evans, X. Duan, *Chem. Commun.* **2010**, *46*, 8654; c) $r = (I_{VV} - G I_{VH}) / (I_{VV} + 2G I_{VH})$, where $G = I_{HV} / I_{HH}$, and I_{VH} stand for the photoluminescence intensity obtained with vertical excitation polarized and horizontal detection polarization, and I_{VH} , I_{HV} , I_{HH} are defined in a similar way.
- [15] A. P.-Z. Clark, K.-F. Shen, Y. F. Rubbin, S. H. Tolbert, *Nano Lett.* **2005**, *5*, 1647.
- [16] T.-Q. Nguyen, J. J. Wu, S. H. Tolbert, B. J. Schwartz, *Adv. Mater.* **2001**, *13*, 609.